Electronic Supplementary Material (ESI) for Dalton Transactions.

Molecular stabilization of chemically exfoliated bare $MnPS_3$ layers

Isaac Brotons-Alcázar,[a] Ramón Torres-Cavanillas[a] Marc Morant-Giner[a], Martin Cvikl[a], Samuel Mañas-Valero[a], Alicia Forment-Aliaga*[a] and Eugenio Coronado.*[a]

Table of contents

Raman Spectra

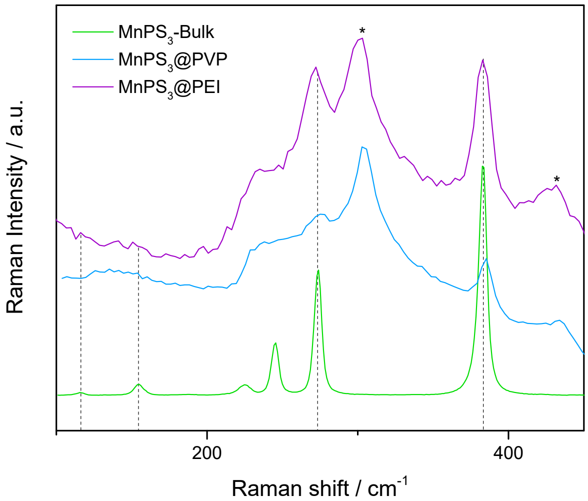

Fig. S1.- Raman spectra of bulk $MnPS_3$, $MnPS_3$@PVP and $MnPS_3$@PEI. Substrate-related peaks are marked as *.

Raman spectra were collected by spin-coating suspensions of different $MnPS_3$-based systems onto Si/SiO_2 substrates. 532 nm laser was employed for performing the measurements.

Table S1.- Raman active modes for $MnPS_3$, $MnPS_3$@PVP and $MnPS_3$@PEI.

Vibration mode	**$MnPS_3$ Bulk**	**$MnPS_3$@PVP**	**$MnPS_3$@PEI**
B_g	115	-	116
A_g	154	-	151
A_g, B_g	224	238	235
A_g	245		
A_g, B_g	274	275	275
Si-O	-	304	303
A_g	383	385	383
Si	-	433	432

ATR-IR Spectra

In **Fig. S2** the main bands of PVP are highlighted pointing out the good agreement of bare PVP bands and those in $MnPS_3$@PVP system. The carbonyl band is shifted to lower energies in the $MnPS_3$@PVP system.

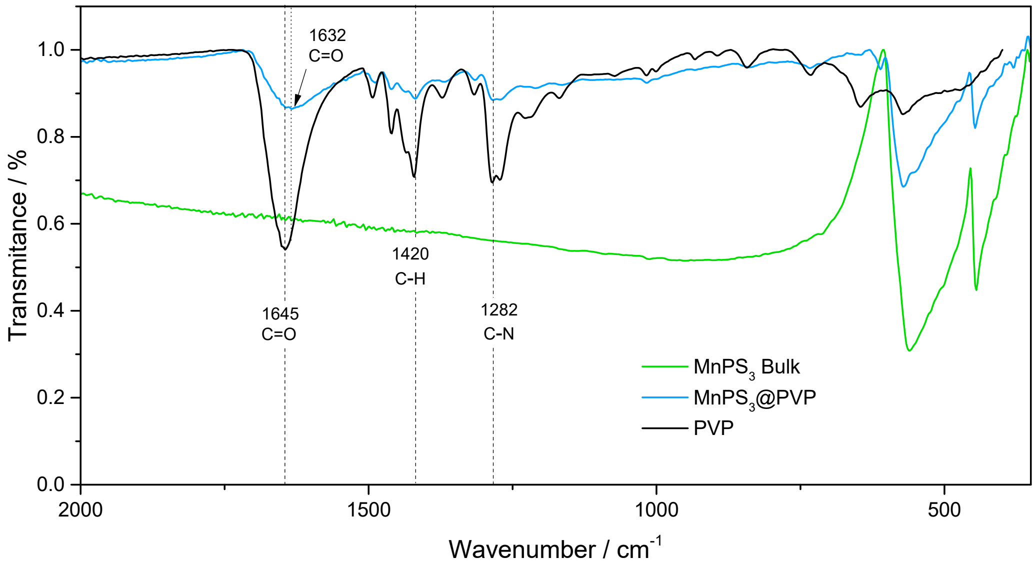

Fig. S2.- Infrared spectra of bulk $MnPS_3$; $MnPS_3$@PVP and commercial PVP

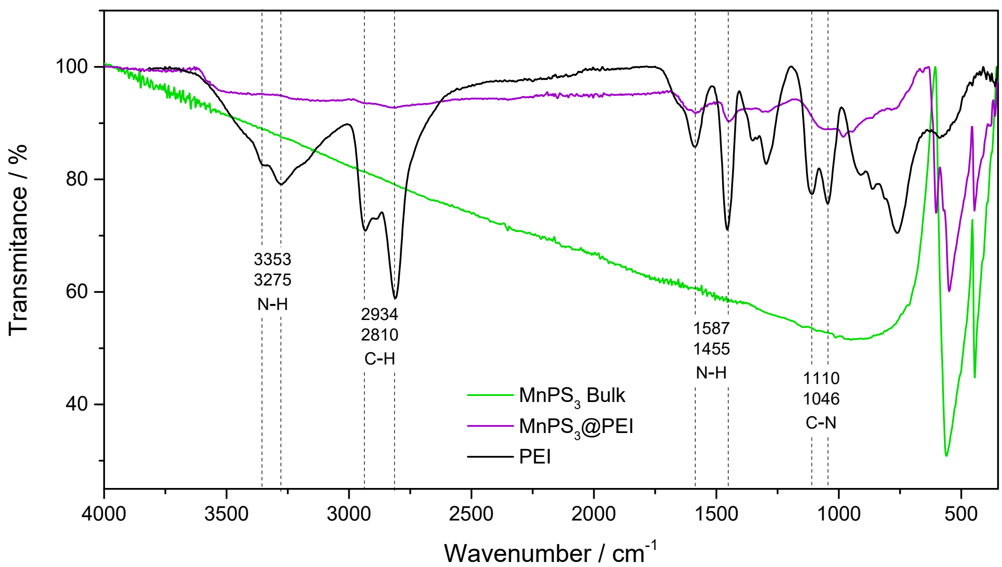

Fig. S3.-Infrared spectra of bulk $MnPS_3$; $MnPS_3$@PEI and commercial PEI

XPS Analysis

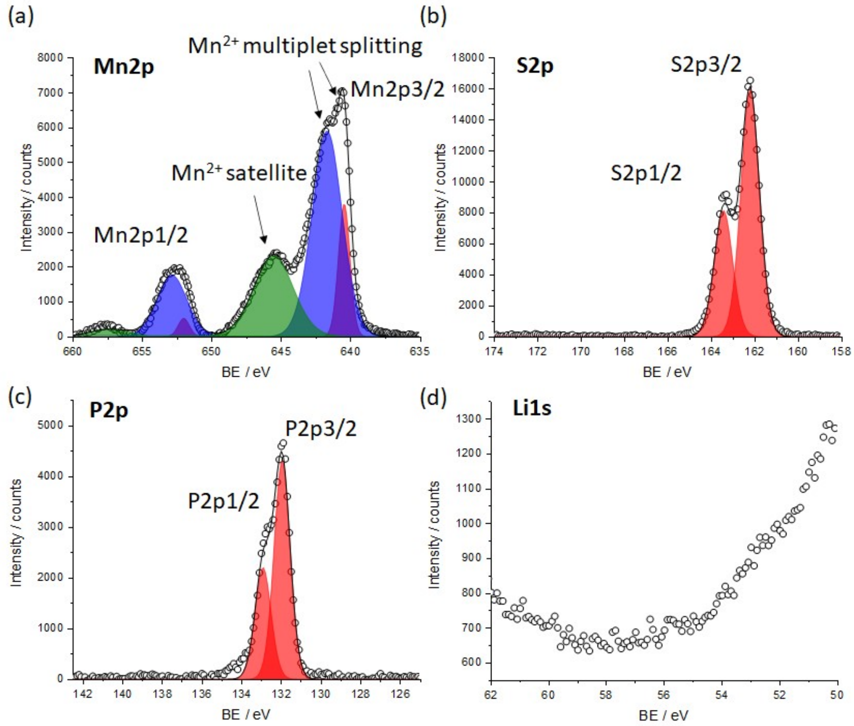

Fig. S4.- a) Mn 2p, b) S2p, c) P2p, and d) Li1s XPS regions of $MnPS_3$@H_2O. Representation of the main peaks (red) (and blue, for Mn splitting) and satellite peaks (green).

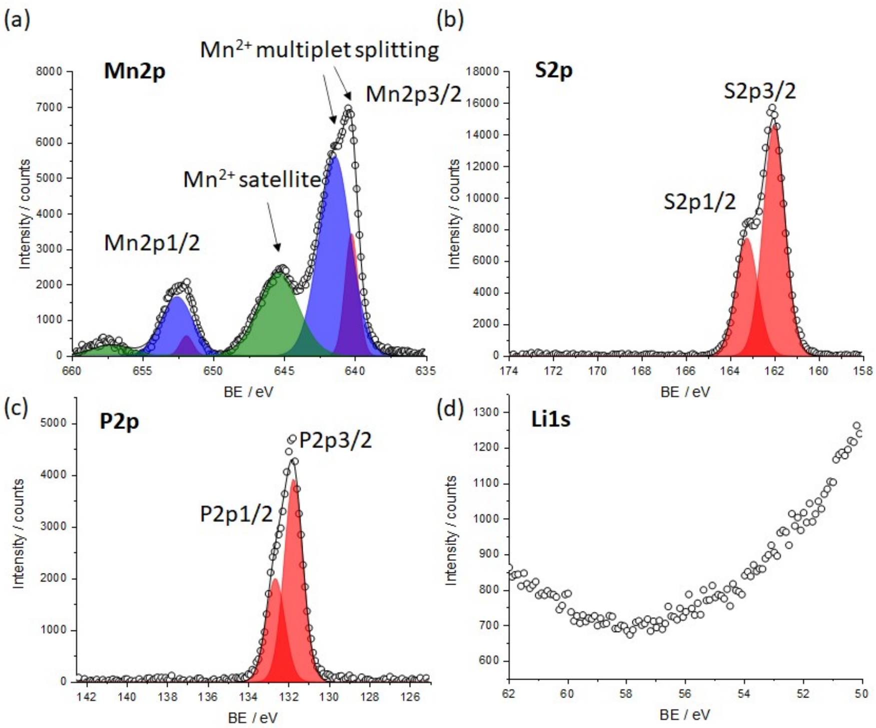

Fig. S5.-a) Mn 2p, b) S2p, c) P2p, and d) Li1s XPS regions of $MnPS_3$@PVP. Representation of the main peaks (red) (and blue, for Mn splitting) and satellite peaks (green).

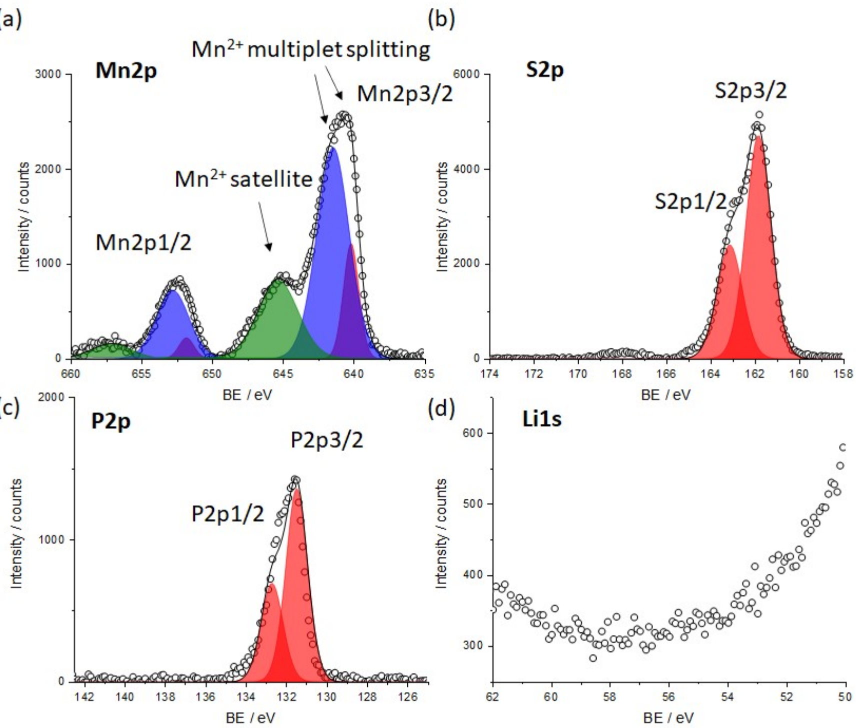

Fig. S6.- a) Mn 2p, b) S2p, c) P2p, and d) Li1s XPS regions of $MnPS_3$@PEI. Representation of the main peaks (red) (and blue, for Mn splitting) and satellite peaks (green).

The electronic signature of the exfoliated material exhibits a complex Mn2p region due to significant multiplet splitting and satellite peaks, Fig S4-S6 (a).[1,2] For all the samples, two sets of bands around 641 eV and 652 eV can be observed, corresponding to the $Mn2p_{3/2}$ and $Mn2p_{1/2}$ levels of Mn^{2+}. For simplicity, each set of bands has been deconvoluted in two main peaks and a satellite.

Also, the presence of S and P is evidenced for the different samples by the appearance of the characteristic S2p and P2p doublets (Fig S4-S6 b and c), while no residual Li^+ from the exfoliation protocol is recorded (Fig S4-S6 d).

Remarkably, the ratio Mn:P:S of the three samples can be quantified from the XPS, estimating values close to the expected 1:1:3 (Table S2), indicating negligible amount of Mn vacancies.

Table S2.- Mn:P:S atomic ratio for $MnPS_3$@H_2O, $MnPS_3$@PVP and $MnPS_3$@PEI

Sample	Ratio Mn:P:S
$MnPS_3$@H_2O	0.9:1.0:2.8
$MnPS_3$@PVP	1.0:1.0:2.9
$MnPS_3$@PEI	1.0:1.0:2.9

Z Potential

The $MnPS_3@H_2O$ presents a negative surface charge after washing alkaline cations out. In the case of $MnPS_3@PVP$, partial reduction of Z potential occurs due to the presence of the capping agent. For $MnPS_3@PEI$, the presence of positively charged amino groups leads to positive surface charge in the system.

Table S3.- Zeta Potential values for $MnPS_3@H_2O$, $MnPS_3@PVP$ and $MnPS_3@PEI$

Sample	Z Potential / mV
$MnPS_3@H_2O$	-43.8 ± 0.4
$MnPS_3@PVP$	-25.5 ± 0.7
$MnPS_3@PEI$	+13.8 ± 0.6

TGA Analysis

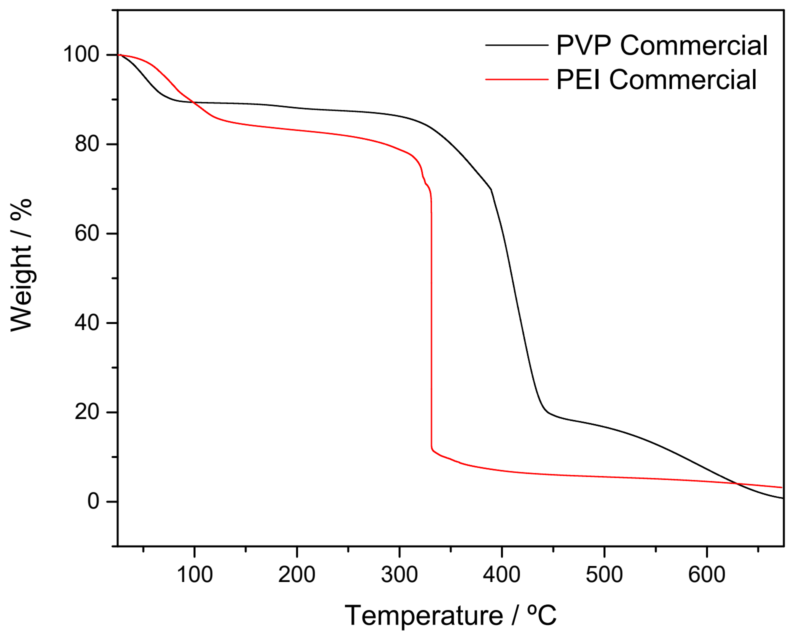

Fig. S7.- TGA analysis under N_2 atmosphere of PVP (Black) and PEI (Red)

PXRD Patterns

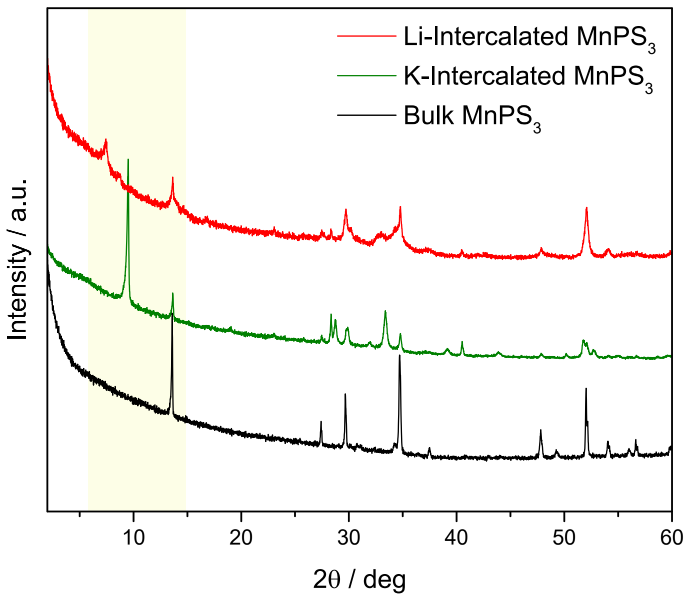

Fig. S8.- XRPD of bulk $MnPS_3$ (Black), K-intercalated $MnPS_3$ (Green) and Li-intercalated $MnPS_3$ (Red). Highlighted area corresponds to the (001) peak displacement.

AFM

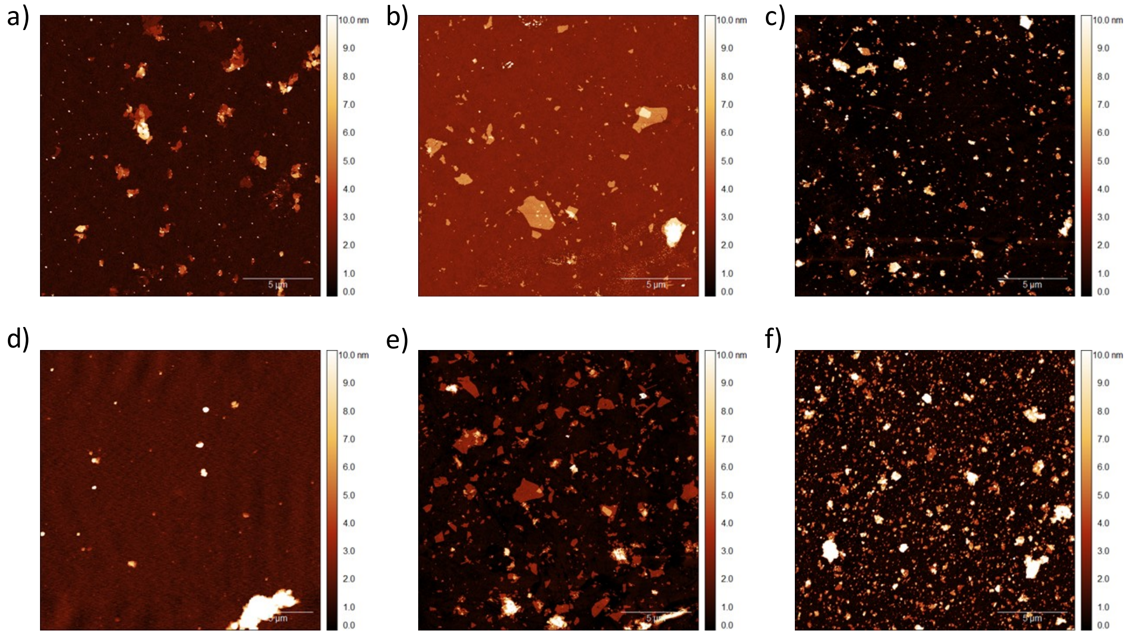

Fig. S9.- Full 20x20 μm^2 AFM topography images of $MnPS_3$@H_2O (a), $MnPS_3$@PVP (b) and $MnPS_3$@PEI (c) spin-coated on Si/SiO_2 substrates right after suspensions were prepared (day 1). Bottom: AFM topography images of $MnPS_3$@H_2O (a), $MnPS_3$@PVP (b) and $MnPS_3$@PEI (c) spin-coated on Si/SiO_2 substrates five days after suspensions used in top images, were prepared (day 5). These images correspond to bigger scope of Fig 4 (a)-(f).

Additional images of AFM have been measured for having an idea of the homogeneity of the samples

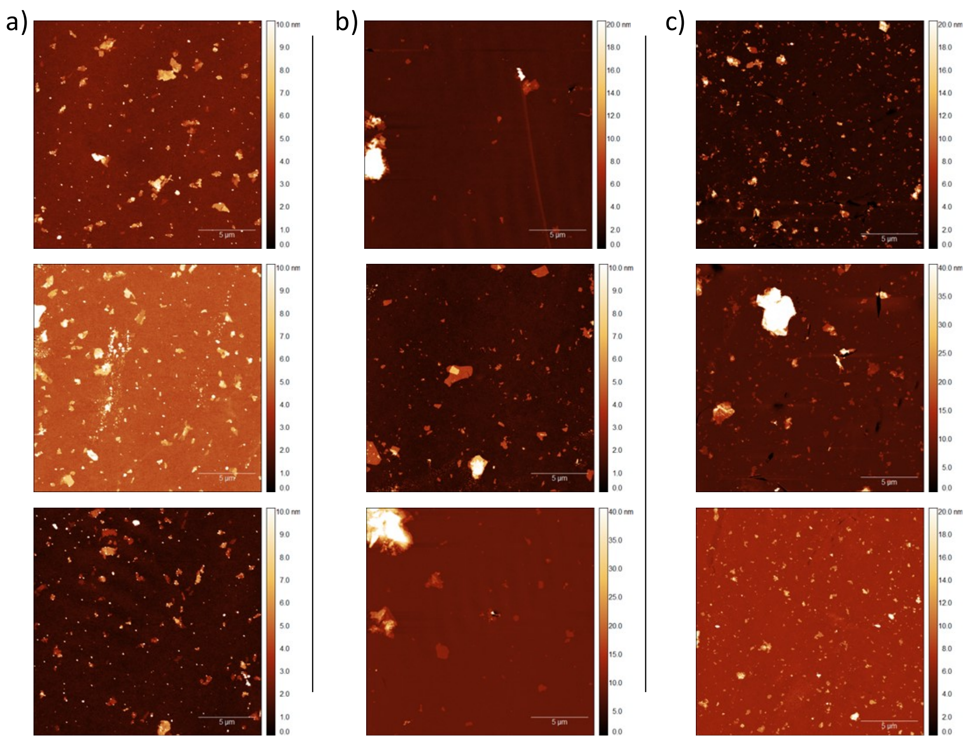

Figure S10.- Additional AFM topography images measured in different spots for a first-day samples of: $MnPS_3$@H_2O (column $MnPS_3$@PVP (column b) and $MnPS_3$@PEI (column c).

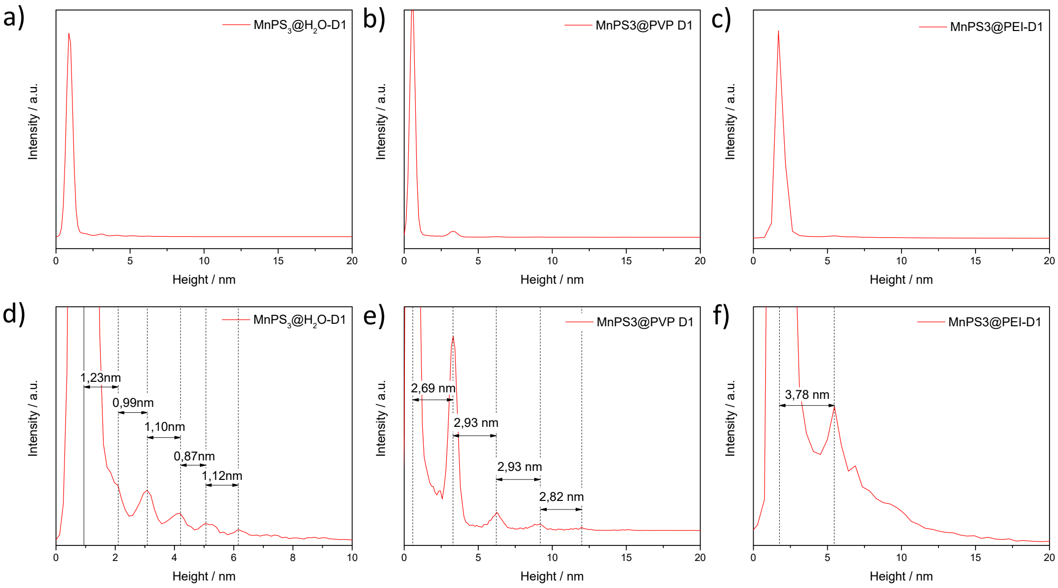

Fig. S11.- Height histograms of first-day samples of a)MnPS$_3$@H$_2$O, b)MnPS$_3$@PVP and c)MnPS$_3$@PEI; d), e) and f) are onsets of a), b) and c), respectively. Histograms (a), (b) and (c) correspond to the pictures presented in Fig S9 (a), (b)

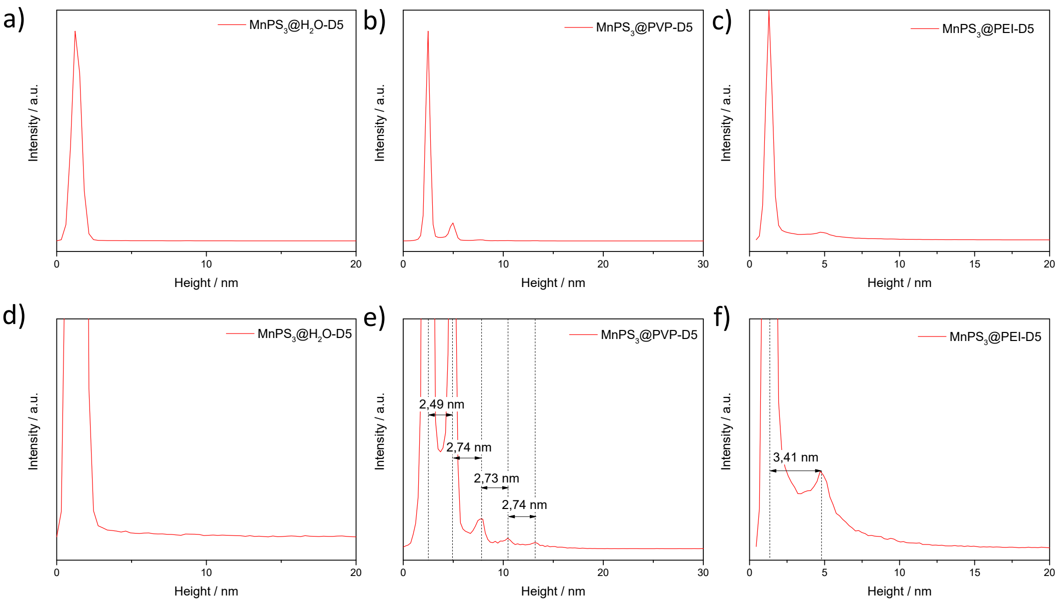

and (c).

Fig. S12.- Height histograms of fifth-day samples of a)MnPS$_3$@H$_2$O, b)MnPS$_3$@PVP and c)MnPS$_3$@PEI; d), e) and f) are onsets of a), b) and c), respectively. Histograms (a), (b) and (c) correspond to the pictures presented in Fig S9 (d), (e) and (f)

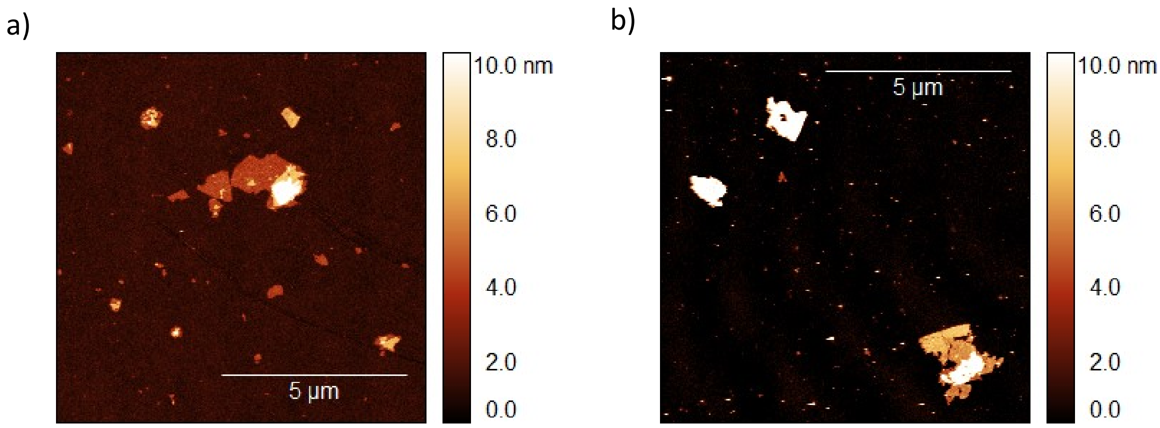

Figure S13.- AFM images taken 35 days after exfoliation of $MnPS_3$@PVP (a) and $MnPS_3$@PEI (b)

MnPS3@PVP Proposed Scheme

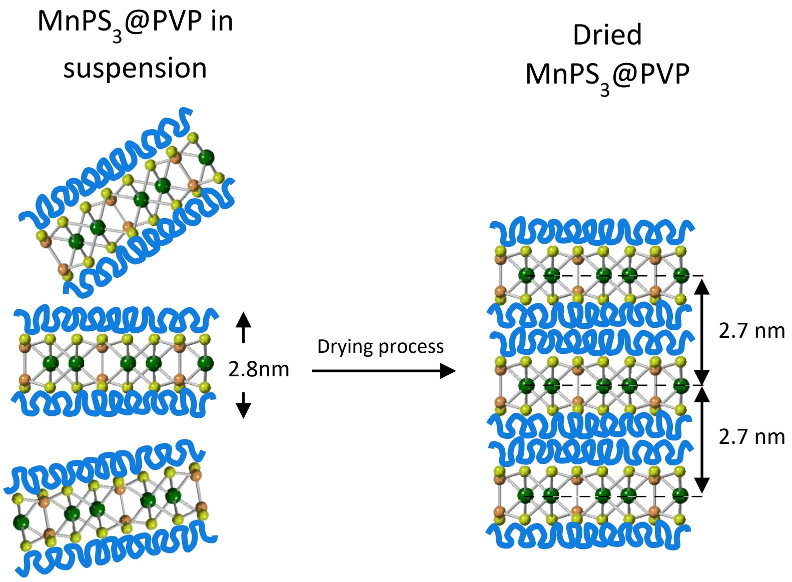

Scheme S1.- Proposed arrangement for $MnPS_3$@PVP layers in suspension and in dried form. Layer thickness determined by AFM (a) and layered structure deduced by XRD (b).

Electrochemistry data

Regarding the efficiency of $MnPS_3$ and other family materials towards HER catalysis it is possible to find several works in literature and the values for overpotential are depicted in Table S4.

Table S4 HER performance achieved for different MPX3 in the present and previous works

Material	η@10mA·cm^{-2} / mV v RHE	Ref
$MnPS_3$@H_2O	525	This work
$MnPS_3$@PVP	738	This work
$MnPS_3$@PEI	532	This work
exf-$MnPS_3$	835	[1]
exf-$MnPSe_3$	640	[1]
Few-Layer-$FePS_3$	211	[2]
Few-Layer $NiPS_3$	297	[3]

All the $MnPS_3$ systems were measured using an electrochemical cell with graphite rod as counter electrode, Ag/AgCl as reference electrode and glassy carbon covered with the target $MnPS_3$ system as working electrode. With this system the values of current density are much lower than the platinum-based system, however, for the sake of comparison, it is worth noting how the tendency of catalytic performance is the same in both systems (Fig. S14).

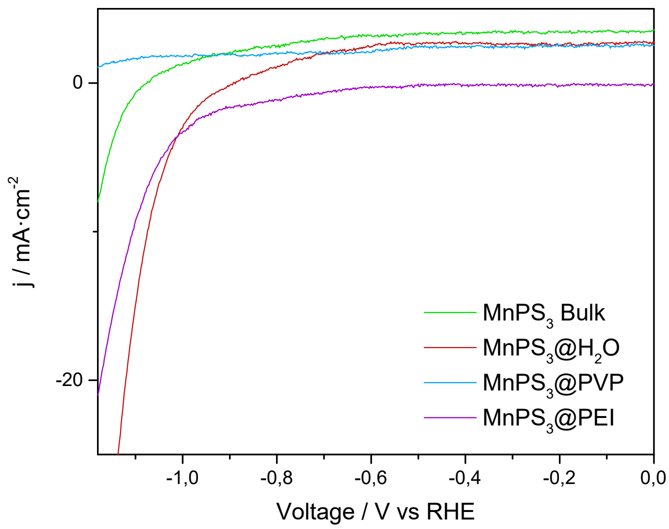

Fig. S14.- LSV measurements for bulk $MnPS_3$, $MnPS_3$@H_2O, $MnPS_3$@PVP and $MnPS_3$@PEI deposited onto glassy carbon working electrode.

Table S5.- Overpotential values for current densities of 10 and 20 mA·cm^{-2} for bulk $MnPS_3$, $MnPS_3$@H_2O, $MnPS_3$@PVP and $MnPS_3$@PEI measured with platinum wire or graphite rod as counter electrode

	Pt as counter electrode		Graphite Rod as counter electrode	
	η@10mA·cm^{-2} /mV	η@20mA·cm^{-2} /mV	η@10mA·cm^{-2} /mV	η@20mA·cm^{-2} /mV
$MnPS_3$ Bulk	-829	-981	-	-
$MnPS_3$@H_2O	-525	-565	-1070	-1120
$MnPS_3$@PVP	-738	-782	-	-
$MnPS_3$@PEI	-532	-601	-1110	-1170